Adaptive Carrier Aggregation for Enhanced Reliability in Multi-Band GEO Satellite Systems

Mohammed Al-Ansi*, Jorge Querol*, Madyan Alsenwi*, Eva Lagunas*, Joan Bas†, Symeon Chatzinotas*
*Interdisciplinary Centre for Security, Reliability and Trust (SnT), University of Luxembourg, Luxembourg
Email: {mohammed.al-ansi, jorge.querol, madyan.alsenwi, eva.lagunas, symeon.chatzinotas}@uni.lu
†Centre Tecnològic de Telecomunicacions de Catalunya (CTTC), SRCOM Research Unit, Spain
Email: joan.bas@cttc.es

***Abstract*—Enhancing reliability in high-throughput satellites (HTS) operating in geostationary orbit (GEO) is critical, particularly under adverse channel conditions. This study investigates the potential of multi-connectivity (MC) enabled by carrier aggregation (CA) to improve the data rate, ensuring a high level of reliability of multi-band Ka/Ku GEO HTS systems. A system and channel model for the multi-band GEO satellite system is developed, and an inter-band CA algorithm is proposed. This algorithm dynamically adjusts the user link transmission scheme based on channel quality and user requirements, ranging from a single Ka-band connectivity to MC, utilizing both bands with CA via packet duplication or packet splitting. The numerical results in various weather scenarios validate the effectiveness of the algorithm, demonstrating significant improvements in system performance, reduced outage probability, and improved overall system reliability. These findings highlight the importance of MC and multi-band technologies in future 6G networks.**

***Index Terms*—6G non-terrestrial network, GEO satellites, multi-band, multi-connectivity, inter-band carrier aggregation, reliability, data rate**

I. Introduction

High-throughput satellites (HTS) and very-high-throughput satellites (VHTS) are essential to improve data transmission in 6G non-terrestrial networks [1]. They are located in geostationary Earth orbit (GEO), medium Earth orbit (MEO), or low Earth orbit (LEO), use multibeam architectures, frequency reuse techniques, and operate across multiple frequency bands, primarily the Ka and Ku bands, to maximize coverage and capacity [2], [3]. Multi-band networks are envisioned as a cornerstone of future 6G systems, providing unprecedented flexibility to meet diverse needs such as extensive connectivity, high data rates, low latency, and broad coverage [4].

Although the high data rate capabilities of H/VHTS systems are well recognized, enhancing their reliability is equally crucial, particularly considering the distinct characteristics of the multiple frequency bands. Despite its relatively wide bandwidth, the Ka-band encounters significant reliability challenges due to its susceptibility to adverse weather conditions, especially rain attenuation. In contrast, the Ku-band is less vulnerable to such environmental factors, although this advantage comes at the cost of lower data rates. This disparity motivates the strategic utilization of each band's unique features to bolster overall system reliability. Moreover, leveraging these characteristics can improve the antijamming capabilities of civilian and government satellite communications [5].

One promising approach to improve reliability in addition to data rate and other advantages is the use of a multi-connectivity (MC) architecture enabled by carrier aggregation (CA) and dual connectivity [6]. MC allows for the concurrent utilization of multiple carriers, thereby enhancing the overall transmission bandwidth of the system. Moreover, these MC technologies improve communication robustness and efficiency by strategically managing packets across various physical channels through packet duplication (PD) and packet splitting (PS). PD improves reliability and reduces latency by sending the same packet over primary and secondary paths, using more bandwidth. In contrast, PS aims to elevate data rates or achieve load balancing by distributing packets over multiple channels. However, this approach relies on the integrity of all channels for successful packet reconstruction, which introduces the potential risk of link failure.

MC technologies have been extensively explored and deployed in terrestrial networks, resulting in significant advances [6], [7]. In parallel, satellite communications are receiving increasing attention in the development of these technologies [8]–[10]. In [11], the carrier-user assignments in GEO systems are optimized through both inter- and intra-transponder CA to improve carrier distribution. In [12], the CA is adapted to variable user demands, optimizing the use of the spectrum. Innovative approaches to load balancing and scheduling [13], together with integrated beam hopping and CA strategies [14], further aim to increase the capacity of the satellite network, spectral efficiency, and quality of service (QOS).
Inspired by the wide features that MC can bring to the satellite domain, this study investigates their advantages through developing CA in multi-band H/VHTS systems. Previous studies have predominantly explored CA within the same band, focusing on improving throughput through PS operation. In contrast, our objective is to enhance data rates and ensure reliability by adaptively leveraging the distinct characteristics of each band, in addition to implementing various packet operation schemes. The main contributions of this study are summarized as follows:

- Develop a multi-band system and channel model that leverages the distinct characteristics of both Ka and Ku bands within a multi-beam structure. This model incorporates dynamic beamforming for the Ka-band to

979-8-3503-6224-4/24/$31.00 ©2024 IEEE

enhance service quality, particularly at the edges of the coverage areas of the beams from the Ku-band.

- Propose an adaptive inter-band carrier aggregation (AICA) algorithm that dynamically maximizes data rates for users under strict reliability constraints. This algorithm adapts based on signal-to-interference-plus-noise ratios (SINRs) and user demands, switching between single connectivity (SC) from the Ka-band and MC cases, including CA with PD and CA with PS.

The organization of the remainder of this paper is as follows: Section II presents the system and channel model for multi-band HTS; Section III explains the formulation of the problem; Section IV describes the proposed AICA algorithm, Section V discusses the numerical results; and Section VI concludes the paper.

II. System and Channel Model for Multi-band GEO HTS

Figure 1 shows a GEO satellite system configured for downlink operations, featuring a multi-beam setup with dual-band functionality designed to accommodate K users with multi-band capabilities. This architecture employs broad-coverage beams in the K_u band (referred to as B_u beams) to provide complete service coverage. The B_u beams are distributed throughout the service area in a uniform and deterministic manner. A layered beam strategy is implemented that incorporates additional beams in the K_a band (denoted as B_a beams), which are intricately nested within each B_u beam. Each B_u beam hosts B_a beams, whose characteristics, such as center alignment, shape, and width, are dynamically modifiable through advanced beamforming technologies [15]. Hence, the B_a beam footprints can be adjusted to improve the QoS of users at the cell edge or other places that target critical communications, such as public safety. Users are randomly distributed within the coverage of each beam, across both bands, ensuring comprehensive coverage where users under a B_a beam (denoted as U_{ka}) also fall within the coverage of at least one B_u beam.

Furthermore, beams within both bands are assigned unique carrier frequencies via a predefined assignment strategy. This includes a four-frequency reuse scheme for the K_u-band to mitigate co-channel interference and a full-frequency reuse approach for the K_a-band, enhancing spectral efficiency. Hence, each beam within the K_u and K_a bands encounters interference from the μ_{Ku} and μ_{Ka} beams, respectively. The B_u beams are organized in a hexagonal grid pattern, with a mandated separation between the center of any given beam and its nearest interfering counterparts, set at more than double the beam's radius. We extend this spatial arrangement to the K_a band through the geographic separation between the beams. The system adopts the 5G New Radio (NR) standard, specifically utilizing zero numerology, and allocates 12 resource blocks to each user. In this analysis, we focus on the m^{th} and n^{th} beams within these bands, identified as the primary beams of interest out of the full set of B_a and B_u beams.

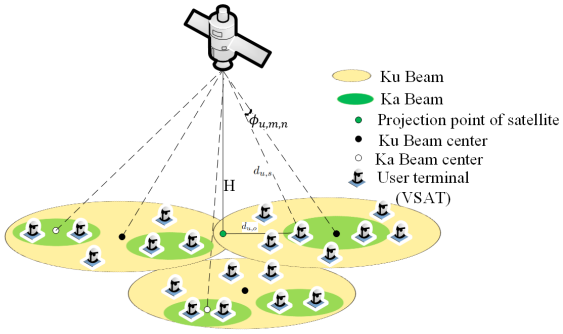

Fig. 1. Schematic diagram for multi-band GEO HTS system

Each u^{th} user located within the coverage area of the m^{th} beam is subject to receiving signals directly from the intended beams in addition to the intra-band interference. Taking into account the distinct physical layers for the K_a and K_u bands, the received signal equations are formulated separately and the received signal for a user u in the K_a and K_u bands are given below. For the K_a band:

$$y_{u,m}^{K_a} = \sqrt{P_t} h_{u,m}^{K_a} x_{u,m}^{K_a} + \sum_{\substack{i=1 \\ i \neq m}}^{\mu_{Ka}} \sqrt{P_t} h_{u,i}^{K_a} x_{u,i}^{K_a} + \omega_u^{K_a}, \quad (1)$$

For the K_u band:

$$y_{u,n}^{K_u} = \sqrt{P_t} h_{u,n}^{K_u} x_{u,n}^{K_u} + \sum_{\substack{j=1 \\ j \neq n}}^{\mu_{Ku}} \sqrt{P_t} h_{u,j}^{K_u} x_{u,j}^{K_u} + \omega_u^{K_u}, \quad (2)$$

where $h_{u,m}^{K_a}$ and $h_{u,n}^{K_u}$ are the channel coefficients from the transmitting beams (m and n) in the K_a and K_u bands, respectively. $x_{u,m}^{K_a}$ and $x_{u,n}^{K_u}$ represent the transmitted signals from the m^{th} and n^{th} beams in the K_a and K_u bands with unit average power, respectively. P_t is the transmit power for each beam, while ω_u^D represent the additive noise at the receiver, where D denotes for the (K_a or K_u), characterized by a zero mean and variance of σ_D^2.

A. Channel Model for Multi-Band HTS

We present a unified channel model for both Ku and Ka-band, where the differentiable characteristics rely on the parameters used within the model (such as rain attenuation coefficient and link attenuation). The channel coefficient received by the u^{th} user from any b^{th} beam in a D^{th} frequency band is expressed as follows [16], [17]:

$$h_{u,b}^D = A_{u,b}^D G_{u,b}^D \quad (3)$$

where $A_{u,b}^D$ and $G_{u,b}^D$ are the link attenuation and small-scale fading for a u^{th} user in the b^{th} beam and D^{th} band, respectively. More specifically, $A_{u,b}^D$ can be defined as:

$$A_{u,b}^D = \frac{\lambda_D}{4\pi d_{u,s}} L_{\text{rain}}^D G_R^D G_{T,b}^D(\phi_{u,b}), \quad (4)$$

where λ_D represents the wavelength for band D, $d_{u,s}$ is the distance between u^{th} user and satellite, and it's equal to

$\sqrt{d_{u,o}^2 + H^2}$, where $d_{u,o}$ is the distance between the u^{th} user and the projection point of the satellite on the Earth's surface, and H is the altitude of the satellite. L_{rain}^D denotes the rain attenuation factor, which can be calculated from the rain rate r (in mm/h) using the power law model: $L_{\text{rain}}^D = \nu_D r^{\iota_D}$ where ν_D and ι_D are the frequency-dependent coefficients defined by ITU-838. G_R^D is the gain from the receiver antenna of the user while and $G_{T,b}^D(\theta_{u,b})$ is the gain from the satellite transmit antenna and it is modeled to include the effects of the location of the user and the beamforming strategies:

$$G_{T,b}^D(\phi_{u,b}) = G_{\text{max}}^D \rho_{u,b}^D(\phi_{u,b}), \tag{5}$$

where G_{max}^D is the maximum transmit antenna gain of the satellite. The normalized beam pattern, $\rho_{u,b}^D(\phi_{u,b})$, is influenced by the user's location, specifically defining the off-axis angle $\phi_{u,b}$ between the center of the b^{th} beam and the location of the u^{th} user. This pattern can be estimated by [18]:

$$\rho_{u,b}^D(\phi_{u,b}) = \left| \frac{J_1(U(\phi_{u,b}))}{2U(\phi_{u,b})} + 36\frac{J_3(U(\phi_{u,b}))}{U^3(\phi_{u,b})} \right| \tag{6}$$

where J_1 and J_3 are the first-kind Bessel functions of orders 1 and 3, respectively. $U(\phi_{u,b})$ can be written as:

$$U(\phi_{u,b}) = \frac{2.07123\sin(\phi_{u,b})}{\sin(\theta_{3dB})} \tag{7}$$

where θ_{3dB} is the angle of the 3dB power loss from the beam center and $\sin(\phi_{u,m})$ can be given by:$\sin(\phi_{u,b}) = \frac{d_{u,b}}{\sqrt{d_{u,b}^2+H^2}}$ where $d_{u,b}$ represents the distance between the u^{th} user and the center of the b^{th} beam. The small-scale fading effect, denoted by $G_{u,b}^D$, is derived from the shadowed Rician distribution, symbolized as $SR(\delta, \Psi, \Omega)$. In this context, δ represents half the average power of the scattered component, Ψ denotes the Nakagami fading coefficient, and Ω signifies the average power of the line-of-sight component. Consequently, the SINR is formulated as follows:

$$\gamma_{u,b}^D = \frac{P_t |A_{u,b}^D|^2 |G_{u,b}^D|^2}{\sum_{i=1, i\neq b}^{\mu_D} P_t |A_{u,i}^D|^2 |G_{u,i}^D|^2 + \sigma_D^2}, \tag{8}$$

Specifically, the SINR for the b^{th} beam within the Ka band, located inside the j^{th} beam of the K_u band, is given as follows:

$$\gamma_{u,b,j}^{K_a} = \frac{P_t |A_{u,b,j}^{K_a}|^2 |G_{u,b,j}^{K_a}|^2}{\sum_{i=1, i\neq b}^{\mu_{K_a}} P_t |A_{u,i,j}^{K_a}|^2 |G_{u,i,j}^{K_a}|^2 + \sigma_{K_a}^2}, \tag{9}$$

III. Problem Formulation

For optimizing efficiency in multi-band satellite communications, it's crucial to adopt a strategic approach that guarantees users receive the best QoS by judiciously exploiting the distinct characteristics of each band. Users with significant bandwidth requirements benefit from the expansive bandwidth of B_a beams. While single connectivity (SC) from the K_a band presents a direct approach, the ultimate data rate hinges on both the allocated K_a band's bandwidth and the SINR. Notably, in scenarios where reliable communication is paramount, especially with rain fading and inter-beam interference, CA with packet duplication (CA-PD) could be a key strategy to enhance link reliability. This method, by transmitting identical data across both bands, leverages the K_u band's resilience and the diversity gained from distinct frequencies and paths, thereby improving the likelihood of successful reception. Nonetheless, indiscriminate utilization of packet duplication may impact spectral efficiency and result in resource waste. Additionally, when links from both bands are highly reliable, and user demand surpasses the rate achievable by a single link, packet splitting between bands and aggregating them through CA with packet splitting (CA-PS) becomes a viable strategy. This scenario underscores the necessity for an optimized or adaptable transmission scheme responsive to dynamic conditions such as weather, user demand, and interference levels. Consequently, we frame the problem as an optimization challenge, aiming to maximize achievable data rates ($\chi_{u,i,j}(\alpha_{u,i,j})$) for users served by multiple bands (represented here by the i^{th} and j^{th} beams) while ensuring robust reliability. The goal is to find the allocated bandwidth ($\beta_{u,i,j}(\alpha_{u,i,j})$) and achievable SINR ($\gamma_{u,i,j}(\alpha_{u,i,j})$) for each user based on the selected transmission scheme. This is done by using decision variables ($\alpha_{u,i,j} \in \{0,1,2\}$) to control the transmission scheme. This can be explained mathematically as follows:

$$\alpha_{u,i,j} = 0, \begin{cases} \beta_{u,i,j}(\alpha_{u,i,j}) = \beta_{u,i,j}^{K_a}, \\ \gamma_{u,i,j}(\alpha_{u,i,j}) = \gamma_{u,i,j}^{K_a} \end{cases} \tag{10}$$

$$\alpha_{u,i,j} = 1, \begin{cases} \beta_{u,i,j}(\alpha_{u,i,j}) = \begin{cases} \beta_{u,i,j}^{K_a}, & \text{if } \gamma_{u,i,j}^{K_a} > \gamma_{u,i,j}^{K_u}, \\ \beta_{u,i,j}^{K_u}, & \text{if } \gamma_{u,i,j}^{K_a} \leq \gamma_{u,i,j}^{K_u} \end{cases} \\ \gamma_{u,i,j}(\alpha_{u,i,j}) = \begin{cases} \gamma_{u,i,j}^{K_a}, & \text{if } \gamma_{u,i,j}^{K_a} > \gamma_{u,i,j}^{K_u}, \\ \gamma_{u,i,j}^{K_u}, & \text{if } \gamma_{u,i,j}^{K_a} \leq \gamma_{u,i,j}^{K_u} \end{cases} \end{cases} \tag{11}$$

$$\alpha_{u,i,j} = 2, \begin{cases} \beta_{u,i,j}(\alpha_{u,i,j}) = \beta_{u,i,j}^{K_a} + \beta_{u,i,j}^{K_u}, \\ \gamma_{u,i,j}(\alpha_{u,i,j}) = \min(\gamma_{u,i,j}^{K_a}, \gamma_{u,i,j}^{K_u}) \end{cases} \tag{12}$$

where, $\alpha_{u,i,j} = 0$ signifies the deployment of SC exclusively via the Ka-band, focusing on a direct allocation approach devoid of CA. On the other hand, $\alpha_{u,i,j} = 1$ when CA-PD is used. In this case, we apply the selection ratio combining (SRC) scheme at the receiver to choose the best link based on SINR measurements. The scenario where $\alpha_{u,i,j} = 2$ denotes the case of using CA-PS. Overall, the optimization problem can be formulated as:

$$\max_{\alpha_{u,i,j}} \quad \sum_{j=1}^{B_u} \sum_{i=1}^{B_a} \sum_{u=1}^{U_{ka}} \chi_{u,i,j}(\alpha_{u,i,j}) \tag{13}$$

subject to

$$C1: \quad \gamma_{u,i,j}(\alpha_{u,i,j}) > \gamma_{\text{out}}$$
$$C2: \quad \chi_{u,i,j}(\alpha_{u,i,j}) >= N_{u,i,j}$$

where $\chi_{u,i,j}(\alpha_{u,i,j}) = \beta_{u,i,j}(\alpha_{u,i,j}) \log_2(1 + \gamma_{u,i,j}(\alpha_{u,i,j}))$ Constraint (C1) ensures that the SINR for each user in the B_a beams exceeds the outage threshold γ_{out}, to improve the

link reliability. The constraint (C2) requires that the data rate for each user $\chi_{u,i,j}(\alpha_{u,i,j})$ be at least equal to the minimum rate requested by that user $N_{u,i,j}$.

IV. Proposed Adaptive inter-band CA (AICA) Algorithm

To optimize the overall system throughput while ensuring the reliability of connections for all users through one of the transmission schemes, as explained in the previous section, we propose the AICA scheme as illustrated in Algorithm 1. AICA dynamically selects the most suitable transmission strategy for each user in the coverage of any B_a beam that is nested inside another B_u beam. The transmission schemes (SC from the Ka band, CA-PD, or CA-PS) are selected based on SINR and user demand. Specifically, SC from the Ka band is preferred for transmissions when the channel quality is high and the achievable rate meets or exceeds user demand, eliminating the necessity for CA. Conversely, CA-PD is employed to bolster QoS, prioritizing reliability even if the current rate falls short of demand in scenarios where the Ka-band's channel quality drops below the outage threshold due to adverse conditions like rain fading or significant interference. Lastly, CA-PS is deployed under conditions where neither of the previous criteria applies, indicating satisfactory link quality from both bands with the primary aim of boosting data rates.

Algorithm 1 Adaptive Inter-band Carrier Aggregation (AICA)

Inputs: γ_{uij}^{Ka}: SINR for u^{th} user in i^{th} beam in Ka band, N_{uij}: demand for u^{th} user, β_{uij}^{Ka}: bandwidth for u^{th} user in i^{th} beam in Ka band, and γ_{out}: outage threshold
for $j = 1$ to B_u **do**
  for $i = 1$ to B_a **do**
    Calculate $\chi_{uij}^{Ka} = \beta_{uij}^{Ka} \log_2(1 + \gamma_{uij}^{Ka})$
    if $\gamma_{uij}^{Ka} > \gamma_{\text{out}}$ **and** $\chi_{uij}^{Ka} > N_{uij}$ **then**
      $\alpha_{uij} = 0$
    else
      if $\gamma_{uij}^{Ka} \leq \gamma_{\text{out}}$ **and** $\chi_{uij}^{Ka} > N_{uij}$ **then**
        $\alpha_{uij} = 1$
      else if $\gamma_{uij}^{Ka} \leq \gamma_{\text{out}}$ **and** $\chi_{uij}^{Ka} \leq N_{uij}$ **then**
        $\alpha_{uij} = 1$
      else
        $\alpha_{uij} = 2$
      end if
    end if
  end for
end for
Output: α_{uij}

V. Numerical Results

This subsection provides the numerical analysis performed to assess the performance of the described multi-band GEO satellite system, as introduced in Section II. Focuses on key performance indicators such as average system throughput, outage probability (OP), and reliability metrics. The OP $P_{out}(\gamma_{\text{out}})$ measures the likelihood that SINR falls below a set threshold, while the reliability $P_{Rel}(\gamma_{\text{out}})$ is defined as the complement of the OP. They can be mathematically represented as:

$$P_{\text{out}}(\gamma_{\text{out}}) = \Pr(\gamma_{u,i,j}(\alpha_{u,i,j}) < \gamma_{\text{out}}) \tag{14}$$

$$P_{\text{Rel}}(\gamma_{\text{out}}) = 1 - P_{\text{out}}(\gamma_{\text{out}}) \tag{15}$$

Also, the throughput estimations are linked to reliability and calculated based on the specified bandwidth and SINR values from Equations 10–12. It can be defined as [16]:

$$T_{\text{thr}} = P_{\text{Rel}}(\gamma_{\text{out}}) \cdot \beta_{u,i,j}(\alpha_{u,i,j}) \log_2 (1 + \gamma_{u,i,j}(\alpha_{u,i,j})) \tag{16}$$

Table I outlines the main simulation parameters. We model a scenario where a single beam from the K_a band ($B_a = 1$) is centrally positioned within each K_u band beam ($B_u = 10$), with beam center randomly determined. User distribution across the beams adheres to a Poisson Point Process (PPP), with an average count of five users per beam, ensuring that the number of users in K_u band beams (U_{Ku}) always equals or exceeds that in K_a band beams (U_{Ka}). Performance outcomes are presented for both clear sky conditions (rain rate $r = 10$ mm/hr) and scenarios involving rain fading ($r = 130$ mm/hr).

TABLE I
Main System Parameters

Parameter	Value
Satellite Altitude (H)	35,786 km
Frequency Band (f_{K_u}/f_{K_a})	14 GHz / 29 GHz
Satellite Antenna Gain (K_u/K_a)	25 dB / 40 dB
Terminal Antenna Gain (K_u/K_a)	10 dB / 15 dB
Beam Bandwidth (K_u/K_a)	36 MHz / 250 MHz
Rain Attenuation (ν, ι) K_u	0.03689, 1.1549
Rain Attenuation (ν, ι) K_a	0.1864, 1.0202
Coverage Radius (K_u/K_a)	150 km / 50 km
θ_{3dB} (K_u/K_a)	0.8° / 0.4°
Polarization	Horizontal / Vertical

Fig. 2 shows the variation in average system throughput as a function of transmission power for various transmission schemes. Notably, transmissions using the Ku band have a lower throughput than other techniques in both clear sky and rain fading, which is due mostly to the band's intrinsic bandwidth limitations and inter-beam interference. Transmissions that only use the Ka band, on the other hand, attain throughput levels comparable to CA-PD, which consistently duplicates packets and AICA techniques. The similarity in performance highlights the Ka band's huge bandwidth advantage over the Ku band. These results also demonstrate that CA-PS, which consistently splits packets, achieves greater throughput than Ku-band transmissions alone but falls short when compared to SC (without CA) from Ka-band transmissions and other CA approaches. This disparity is mostly owing to bandwidth differences between the two bands as well as the SINR's crucial role in restricting performance results. Specifically, packet splitting is based on the link quality of both bands,

with the user's attainable rate limited by the lower SINR of the two links. Furthermore, the CA with the PD scenario revealed greater throughput than the PS instance. This increase is due to SINR enhancements produced using MRC, which enable considerable diversity benefits.

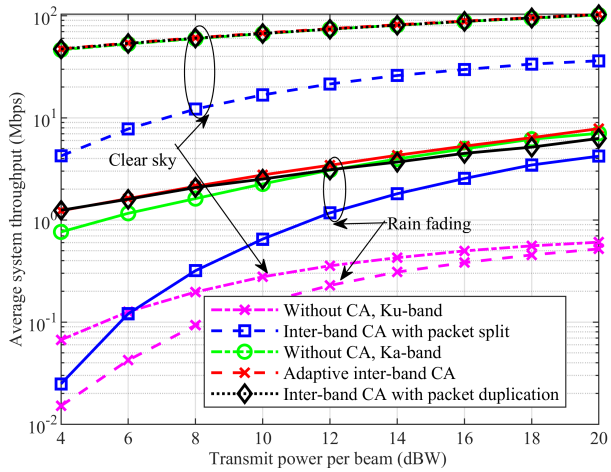

Fig. 2. Average system throughput (Mbps) versus transmit power per beam, where $\gamma_{\text{out}} = 2\,\text{dB}$

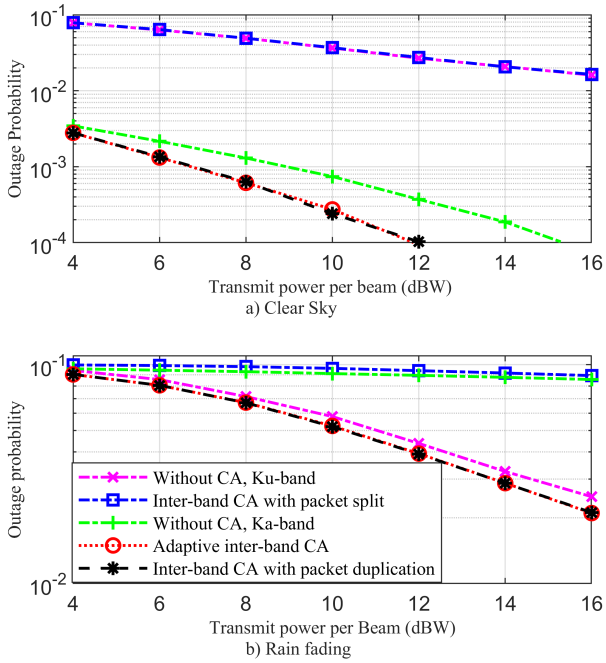

Fig. 3. Outage probability vs. transmit power beam under a) Clear sky and b) Rain fading, R (130 mm/h).

Fig. 3 shows an examination of the OP as a function of transmit power to assess the resilience of the system under different schemes selected. This chart shows a distinct drop in outage likelihood as transmit power increases, demonstrating an obvious relationship between power levels and the link's resistance to failure. Most importantly, the use of adaptive CA has emerged as a critical method to reduce OP in a variety of weather conditions. This flexibility is critical to dynamically maximize the use of available spectrum resources, lowering the chance of outages even in harsh situations. The impact of rain fading on different transmission methods is especially notable. Non-CA transmissions in the Ka-band and CA-PS are more susceptible to rain fading, owing to the intrinsic susceptibility of higher frequency bands to atmospheric attenuation.

In contrast, the findings demonstrate the considerable resilience of the Ku band against rain-induced fading, proving its applicability to preserve the quality of the connection in precipitation-affected circumstances. This resilience is due to the lower frequency of the Ku band, which is less affected by rain fading than other higher frequency bands.

Fig. 4 investigates reliability vs. rainfall intensity and captures the distinct implications of climatic variables on various transmission mechanisms, complementing and expanding on the insights gained from Figures 2 and 3. It clearly shows the increased reliability of adaptive CA and CA-PD versus rain rates, validating their usefulness in combating rain fade. Fig. 5 supplements previous discussions by plotting throughput fluctuations versus rain rates, highlighting the effect of reliability restrictions on CA-PS. As seen in Figure 2, CA-PS does not meet the throughput levels of non-CA (Ka-band) and CA-PD when the rain fades. Meanwhile, adaptive CA, CA-PD and non-CA (Ka band) retain greater throughput, although

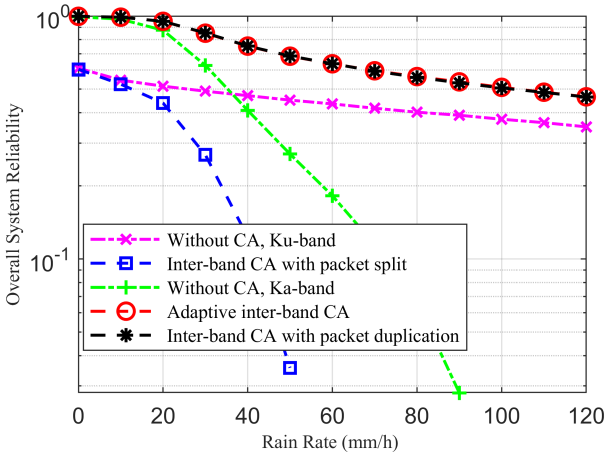

Fig. 4. Reliability vs. rain rate, where $\gamma_{\text{out}} = 2\,\text{dB}$, $P_t = 10dBW$.

with a noticeable reduction under heavier rain circumstances, emphasizing the need for strategic transmission choices in weather-affected situations.

Looking at reliability versus different outage thresholds, Fig. 6 highlights the difficulties of raising these thresholds: As they increase, the reliability of the system worsens. This characteristic underlines the adaptive CA and CA-PD schemes' capacity to maintain high levels of reliability throughout a wide range of thresholds, as opposed to the reduced effectiveness of non-CA (Ka band) and CA-PS systems, which are principally restricted by the Ka band's link limitations.

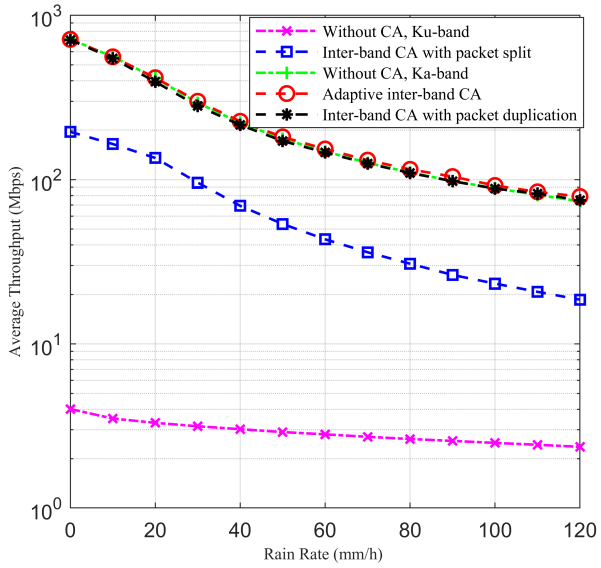

Fig. 5. Throughput vs. rain rate, where $\gamma_{\text{out}} = 2\,\text{dB}$, $P_t = 10dBW$.

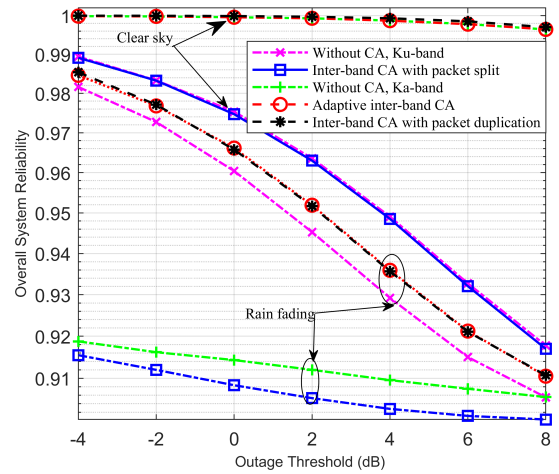

Fig. 6. Reliability vs. outage threshold, where $P_t = 10\text{dBW}$.

VI. Conclusion

This study demonstrates the potential of multi-connectivity (MC) enabled by carrier aggregation (CA) to enhance the reliability and data rates of multi-band high-throughput satellite systems in geostationary Earth orbit. By developing a system and channel model that leverages the unique characteristics of the Ka and Ku bands within a multi-beam architecture, and proposing an adaptive Inter-band CA (AICA) algorithm, we optimize data rates and reliability based on signal-to-interference-plus-noise ratios and user demands. Numerical results validate the effectiveness of the AICA algorithm under various conditions, showing significant improvements in system performance, reduced outage probability, and improved overall reliability. These findings underscore the critical role of multi-band and MC strategies in future 6G networks, highlighting their importance for reliable and high-capacity satellite communication systems.

VII. Acknowledgment

This work has been supported by the project TRANTOR, which has received funding from the European Union's Horizon Europe research and innovation program under grant agreement No. 101081983

References

[1] A. I. Perez-Neira, M. A. Vazquez, M. R. B. Shankar, S. Maleki, and S. Chatzinotas, "Signal processing for high-throughput satellites: Challenges in new interference-limited scenarios," *IEEE Signal Process. Mag.*, vol. 36, no. 4, pp. 112–131, 2019.

[2] J. Ran, Y. Wu, C. Jin, P. Zhang, and W. Wang, "Dual-band multipolarized aperture-shared antenna array for ku-/ka-band satellite communication," *IEEE Trans. Antennas Propag.*, vol. 71, no. 5, pp. 3882–3893, 2023.

[3] M. Holmes, "Orbit communication systems revolutionizes connectivity with multi-band and multi-orbit satcom and earth observation systems," July 2023. Accessed: 2024-06-11.

[4] S. Aboagye, M. A. Saeidi, H. Tabassum, Y. Tayyar, E. Hossain, H.-C. Yang, and M.-S. Alouini, "Multi-band wireless communication networks: Fundamentals, challenges, and resource allocation," *IEEE Trans. Com.*, 2024.

[5] P. Tedeschi, S. Sciancalepore, and R. Di Pietro, "Satellite-based communications security: A survey of threats, solutions, and research challenges," *Comput. Netw.*, vol. 216, p. 109246, 2022.

[6] M.-T. Suer, C. Thein, H. Tchouankem, and L. Wolf, "Multi-connectivity as an enabler for reliable low latency communications—an overview," *IEEE Com. Surv. Tutorials*, vol. 22, no. 1, pp. 156–169, 2019.

[7] Nidhi, B. Khan, A. Mihovska, R. Prasad, and F. J. Velez, "A study on cross-carrier scheduler for carrier aggregation in beyond 5g networks," in *AT-AP-RASC*, 2022.

[8] M. Majamaa, "Toward multi-connectivity in beyond 5g non-terrestrial networks: Challenges and possible solutions," *IEEE Com. Mag.*, 2024.

[9] M. Al-Ansi, J. Querol, E. Lagunas, and S. Chatzinotas, "Single-and multi-connectivity for multi-satellite 6g communication networks," in *Proc. ICSSC*, 2023.

[10] M. N. Dazhi, H. Al-Hraishawi, M. R. B. Shankar, S. Chatzinotas, and B. Ottersten, "Energy-efficient service-aware multi-connectivity scheduler for uplink multi-layer non-terrestrial networks," *IEEE Trans. Green Commun. Netw.*, vol. 7, no. 3, pp. 1326–1341, 2023.

[11] M. G. Kibria, E. Lagunas, N. Maturo, D. Spano, H. Al-Hraishawi, and S. Chatzinotas, "Carrier aggregation in multi-beam high throughput satellite systems," in *Proc. IEEE GLOBECOM*, pp. 1–6, 2019.

[12] E. Lagunas, M. G. Kibria, H. Al-Hraishawi, N. Maturo, and S. Chatzinotas, "Dealing with non-uniform demands in flexible geo satellites: The carrier aggregation perspective," in *Proc. ASMS/SPSC*, pp. 1–5, 2020.

[13] H. Al-Hraishawi, N. Maturo, E. Lagunas, and S. Chatzinotas, "Scheduling design and performance analysis of carrier aggregation in satellite communication systems," *IEEE Trans. Veh. Tech.*, vol. 70, no. 8, pp. 7845–7857, 2021.

[14] M. G. Kibria, H. Al-Hraishawi, E. Lagunas, S. Chatzinotas, and B. Ottersten, "Joint beam hopping and carrier aggregation in high throughput multibeam satellite systems," *IEEE Access*, vol. 10, 2022.

[15] H. Chaker, H. Chougrani, W. A. Martins, S. Chatzinotas, and J. Grotz, "Matching traffic demand in geo multibeam satellites: The joint use of dynamic beamforming and precoding under practical constraints," *IEEE Trans. Broad.*, vol. 68, no. 4, pp. 819–833, 2022.

[16] D.-H. Na, K.-H. Park, Y.-C. Ko, and M.-S. Alouini, "Performance analysis of satellite communication systems with randomly located ground users," *IEEE Trans. Wireless Com.*, vol. 21, no. 1, 2021.

[17] M. Yuan, Y. Gu, and B. Xia, "Downlink performance analysis of the multi-beam geo satellite communication systems," in *Proc. WCSP*, 2021.

[18] G. Zheng, S. Chatzinotas, and B. Ottersten, "Generic optimization of linear precoding in multibeam satellite systems," *IEEE Trans. Wireless Comm.*, vol. 11, no. 6, pp. 2308–2320, 2012.